Açık kaynak kodlu SU2 yazılımı kullanılarak 155 mm mühimmat için gerçek ve simülasyon aerodinamik katsayılarının karşılaştırılması

Comparison of real and simulation aerodynamic coefficients for 155 mm ammunition using open-source code SU2 software

Yazarlar (Authors): *Ahmet Ali SERTKAYA[1], Can ÇALIŞKAN[2], Süleyman NEŞELİ[3]*

ORCID[1]: 0000-0002-9884-445X

ORCID[2]: 0000-0002-6338-2718

ORCID[3]: 0000-0003-1553-581X

Comparison of Real and Simulation Aerodynamic Coefficients for 155 mm Ammunition Using Open-Source Code SU2 Software

Highlights

- ❖ *The comparison of real and simulative aerodynamic coefficients (density, energy, pressure, temperature changes, and drag coefficients) acting on 155 mm long-range howitzer ammunition with the computational flow dynamics software SU2.*
- ❖ *RANS equations, which are operationally simplified variations of the N-S flow solver, were used in the simulations.*
- ❖ *0.7 and 2.8 Mach numbers used in the study for simulation.*
- ❖ *It was determined that drag coefficient increases sharply between Mach 0.7 and 1.3*
- ❖ *The percentage overlap values found by the proportional comparison of the drag coefficient values obtained as a result of the real and simulation in the same Mach numbers were examined, it was determined that the overlap at Mach 0.7 was 83.33%, and 100 ± 2% in the other Mach numbers.*

Graphical Abstract

Figure shows a plot of the drag coefficient with respect to the Mach number from 0.7 to 2.8 at an angle of attack of zero.
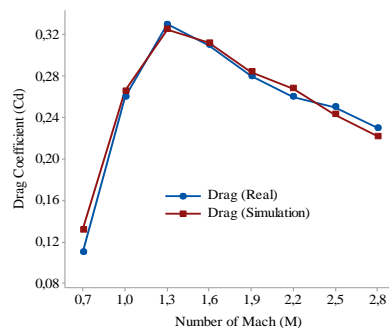

Figure Drag force coefficient (C_d) as a function of Mach number.

Aim

In this study, density, energy, pressure, temperature changes, and drag coefficients occurring during the trajectory of movement for a 155 mm ammunition shell were simulated with the computational flow dynamics software Stanford University Unstructured (SU2).

Design & Methodology

Reynolds-Averaged Navier-Stokes (RANS) equations, which are operationally simplified variations of the Navier-Stokes (N-S) flow solver, were used in the simulations. The Reynolds number based on the velocity was between 1.65x107 to 6.5x107 according to the Mach (M) number between 0.7 to 2.8 in the present simulation.

Originality

The Free Computer-Aided Design (FreeCAD) program was used for geometrical drawings of the ammunition, the Geometry Description, Meshing, Solving, and Post-Processing (GMSH) software for mesh operations, and the Shear Stress Transport (SST) turbulence model to create a compressible finite volume.

Findings

For the drag coefficient values, density-based N-S equations for Mach 1.3 and 2.8 and pressure-based N-S equations for Mach 0.7 and 1.0 were found to give more realistic results.The density, energy, pressure, and temperature change rates increased parallel to each other due to the increase in Mach values at subsonic and supersonic speeds.

Conclusion

All Mach numbers, it was observed that the pressure and temperature were higher in the front of the ammunition. By choosing a rounded design instead of the blunt design of the bullet nose, the airflow can be relieved, and pressure and temperature can be reduced. In this way, a longer range can be achieved as the drag coefficient decreases.

Declaration of Ethical Standards

The authors of this article declare that the materials and methods used in this study do not require ethical committee permission and/or legal-special permission.

Açık Kaynak Kodlu SU2 Yazılımı Kullanılarak 155 mm Mühimmat İçin Gerçek ve Simülasyon Aerodinamik Katsayılarının Karşılaştırılması

Araştırma Makalesi / Research Article

Ahmet Ali SERTKAYA[a,*], Can ÇALIŞKAN[b], Süleyman NEŞELI[a]

[a] Selçuk University, Department of Mechanical Engineering, Konya/Turkey.
[b] Ministry of National Defense, Firing Test and Evaluation Center, Konya/Turkey.

ÖZ

Bu çalışmada, 155 mm'lik bir mühimmat mermisinin hareket yörüngesi boyunca meydana gelen yoğunluk, enerji, basınç, sıcaklık değişimleri ve sürükleme katsayıları Stanford University Unstructured (SU2) hesaplamalı akış dinamiği yazılımı ile simüle edilmiştir. Simülasyonlarda Navier-Stokes (N-S) akış çözücüsünün operasyonel olarak basitleştirilmiş varyasyonları olan Reynolds-Averaged Navier-Stokes (RANS) denklemleri kullanılmıştır. Hıza dayalı Reynolds sayısı, mevcut simülasyonda 0,7 ila 2,8 arasındaki Mach (M) sayısına göre $1,65 \times 10^7$ ila $6,5 \times 10^7$ arasındaydı. Sürükleme katsayıları 0.7 M'den 2.8 M'ye kadar her Mach 0.3 artışı için ayrı ayrı elde edilmiştir. Mühimmatın geometrik çizimleri için Free Computer-Aided Design (FreeCAD) programı, ağ işlemleri için Geometry Description, Meshing, Solving, and Post-Processing (GMSH) yazılımı ve sıkıştırılabilir sonlu hacim oluşturmak için Shear Stress Transport (SST) türbülans modeli kullanılmıştır. Ayrıca, hücum açısı olarak 0 derece kullanılmıştır. Simülasyonlardan elde edilen aerodinamik katsayı yüzde değişimlerinin tahmini için R^2 değerine göre geçerliliği en yüksek olan üstel denklemler oluşturulmuştur. Ayrıca hesaplanan sürükleme katsayıları gerçek değerler ile karşılaştırılmış ve aralarında iyi bir uyum olduğu gözlenlenmiştir.

Anahtar Kelimeler: Aerodinamik katsayılar, RANS, SST, SU2.

Comparison of Real and Simulation Aerodynamic Coefficients for 155 mm Ammunition Using Open-Source Code SU2 Software

ABSTRACT

In this study, density, energy, pressure, temperature changes, and drag coefficients occurring during the trajectory of movement for a 155 mm ammunition shell were simulated with the computational flow dynamics software Stanford University Unstructured (SU2). Reynolds-Averaged Navier-Stokes (RANS) equations, which are operationally simplified variations of the Navier-Stokes (N-S) flow solver, were used in the simulations. The Reynolds number based on the velocity was between 1.65×10^7 to 6.5×10^7 according to the Mach (M) number between 0.7 to 2.8 in the present simulation. The drag coefficients from 0.7 M to 2.8 M were obtained separately for each Mach 0.3 increase. The Free Computer-Aided Design (FreeCAD) program was used for geometrical drawings of the ammunition, the Geometry Description, Meshing, Solving, and Post-Processing (GMSH) software for mesh operations, and the Shear Stress Transport (SST) turbulence model to create a compressible finite volume. As well, 0 degrees was used as the angle of attack. For estimation of the aerodynamic coefficient percentage changes obtained from the simulations, exponential equations with the highest validity based on the R^2 value were created. In addition, the calculated drag coefficients were compared with the actual values and a good fit was observed between them.

Keywords: Aerodynamic coefficients, RANS, SST, SU2.

1. INTRODUCTION

The most important research and developments in the defense industry include studies on weapon systems [1-4]. Particularly in initial studies on ammunition, it was assumed that the force exerted on the ammunition is only in the direction of Cartesian coordinate axes (x, y, z). Today the presence of moment factors around these axes is also considered in system designs. During the movement of ammunition through the air, multi-directional forces and moment factors affect the ammunition's stability, range, and destructive effect on the target. In terms of military purposes, during the design stage of ammunition, the most important focus is the ammunition's ability to reach targets at greater distances and achieve the desired destruction without endangering the users or equipment. An important factor in increasing range and effectiveness is to decrease the drag force caused by the friction that occurs when ammunition comes in contact with the air. This friction

force includes a dimensionless coefficient called the drag coefficient, which varies depending on the geometry of the object in the air environment and the type of fluid the object is in. The drag coefficient is the level of resistance shown by the fluid in the direction opposite to the direction of motion of the body moving in the fluid.

When designing wingless ammunition, especially for use in howitzers or similar military vehicles, the aim is to have a low drag force and therefore a low drag coefficient. These troublesome factors for designers initially required the production of separate prototypes for each design, followed by testing and evaluating each result, which in some cases could be impossible due to cost and technological inadequacies. However, thanks to ever-evolving technology, the production, and testing of prototypes today are done using computational fluid dynamics (CFD) systems, easily minimizing trial time and costs. In addition, because of computer simulations, determining the forces and moments acting on ammunition becomes much simpler. For this purpose, software such as ANSYS, OpenFOAM, ElmerFEM, and SU2 are used in the industry to calculate the aerodynamic coefficients of solids moving in fluid environments such as aerospace and submarine.

In the design industry, as an open-source package, SU2 is uniquely positioned to serve as an example to computational scientists around the world on how one can achieve high-performance and scalability on advanced hardware architectures. The open-source platform can be used as an artificial testing area for various code optimization strategies and studies on the implications of algorithmic choices. Furthermore, its open-source nature allows for rapid and effective technology transfer to the community [5]. The SU2 software tools written in C++ for performing CFD analysis and design make this open-source project specifically suited for the analysis of partial differential equations (PDEs) and PDE-constrained optimization problems on unstructured meshes with state-of-the-art numerical methods, and aerodynamic shape design. Although initial applications were mostly in aerodynamics, through the initiative of users and developers around the world, SU2 is now being used for a wide variety of problems beyond aeronautics, including but not limited to automotive, naval, and renewable energy applications [6]. The treatment of the open-source SU2 suite makes the work done in this research extensible to the larger CFD community for performing similar optimizations on modern, highly parallel architectures.

As lower costs have contributed to the increase in computing power, and as simulation algorithms have become more fully developed, CFD has been increasingly adopted to predict the aerodynamic coefficients of projectiles. The CFD methodology accurately predicts the aerodynamic coefficient, including static and dynamic load, and improves performance through analysis of the flow field around the projectile and its control surfaces [7].

Suvanjumrat [8] compared turbulence models of the NACA 0015 type aircraft wing profile design using OpenFOAM. The Spart Allmaras, Wilcox k-w, and Menter SST models were used for comparisons. Semi Implicit Method for Pressure Linked Equations (SIMPLE) was used to effectively solve the zero-pressure gradient problem of the pressure-velocity coupling. , To compares the physical quantity, the drag (CD) and lift coefficients (CL) were obtained and then compared to the coefficients obtained as a result of the experiments carried out in the wind tunnel. A Reynolds number between 1.6x105 and 3.6x105 was arranged to investigate the NACA0015 airfoil with a large range angle of attack from 0° to 20° when immersed in low wind speeds and turbulent flow. The most suitable turbulence model was the Menter SST model which employed the SIMPLE algorithm and LUD scheme in its solution. These CFD results lowered the stall angle of attack and had average errors of CL and CD which were less than 13.15% and 22.36%, respectively.

Patel et al. [9] investigated drag and lift force values by using CFD methodology and also validated their results through experiments using wind tunnel testing. They analyzed two-dimensional subsonic flow over a NACA 0012 airfoil at various angles of attack using a Reynolds number of 3×106. Based on the CFD analysis of the flow over the airfoil, they concluded that at zero degrees of angles of attack, there no lift force is generated; and if the amount of lift force and value of lift coefficient increases then the angle of attack also increases. Their results showed that the amount of drag force and drag coefficient value increased, but the incremental amounts of each are lower compared to lift force.

Shen et al. [10] performed hypersonic aerodynamic analysis to improve the basic aerodynamic properties of projectile configuration with an electromagnetic gun (EM). Based on the theory of projectile aerodynamics, the static margin and pendulum motion analysis frameworks were set up to assess the flight stability of the new airframe configuration. With a steady-state CFD simulation, the basic density, pressure, and velocity contours of the electromagnetic gun projectile flow field at Mach 5.0, 6.0, and 7.0 (angle of attack is 0) were analyzed. Furthermore, the static margin values were enhanced dramatically for the electromagnetic gun projectile with configuration optimization. Drag, lift, and pitch property variations were all illustrated with the changes of Mach number and angle of attack. They found that the configuration optimized projectile, launched from the EM gun at Mach 5.0 to 7.0, acted in a much more stable way than projectiles with regular aerodynamic layouts.

Weinatch [11] conducted a CFD analysis considering the orbital performance, motion stability, and vibrational movements of bullets for the prediction of free flight motion trajectories. For this purpose, firing data of a projectile moving at high speed under normal conditions was solved by the thin-layer Navier-Stokes method, and the simulation was compared with real physical

experiments. As a result of the experiments, the author observed that there was good harmony between the orbit of the mathematical model made with the coefficients obtained from the CFD and the experiment.

Merda and Magier [12] found trajectory and aerodynamic coefficients of the supersonic mortar shell developed for the army with the trajectory tracking radar. Ansys Fluent software was used to compare the acquired data to aerodynamic coefficients. Experimental data were obtained by firing with a 45° nose angle and a maximum speed of 500 m/s and a range of 10.000 m. Analysis of radar data showed drag fluctuations at low velocities of flight (0.5-0.8 Ma). The CFD method was used to calculate the center of force and stability moments. Drag coefficients at different yaw angles were also estimated. That data was used to model the yaw of projectiles to compare with experimental data. As a result of the comparisons, they stated that CFD simulations in the development of new types of bullets are both faster and more cost-effective than other methods.

Boa at. al. [13] examined forces and moments affecting ammunition along with trajectory via simulation with STAR-CCM+. Mathematical fly path codes that would characterize the orbit of the ammunition were carried out in Mathematica and the solution was verified with the PRODAS program. As a result of these calculations, the nose angle was revised in the design of the ammunition and the changes in aerodynamic forces were examined. According to the results obtained, it was stated that the range and orbital stability were highly influenced by changing the nose angles. They stated that ammunition geometry changes may result in unstable ammunition performance.

Another computational study was undertaken by Silton [14] to predict the static-aerodynamic, Magnus-moment, and roll-damping coefficients of a standard spinning projectile using a single, modern, unstructured Navier–Stokes flow solver. Numerical results without engraving and semi-empirical results were obtained for a wide range of Mach numbers including subsonic, transonic, and supersonic flight regimes. Effects of 0-, 2- and 5-degree angles of attack were investigated. Flow field characteristics of each flight regime were briefly explored. A comparison of coefficients calculated from the CFD results was made to both the experimental range data as well as the semi-empirical aero-prediction code results with some success. Good predictive capabilities were found for the static aerodynamic coefficients throughout all of the flight regimes. Discrepancies arose between the computational results and the experimental results for the Magnus moment and roll-damping coefficients due in part to the lack of engraving on the computational model.

Rafeie and Teymourtash [15] tried a numerical solution of the Navier-Stokes equations by considering the Jameson method in the transonic flow regime over three air gun pellets. The considered pellets were all of the same 4.5 mm calibers, but had different nose shapes; they

were axisymmetric projectiles of three basic types. After these pellets were modeled geometrically, the Navier-Stokes equations as the governing equations of the flow field around the pellets were solved. Computed aerodynamic results were used to dynamically analyze the trajectories of the projectiles. The variation of the drag coefficient by Mach number of the free stream flow, which is a key point for the dynamic analysis of the projectile motion, was obtained. Relying on these analyses, from both aerodynamic and dynamic points of view, the round-nose pellet in a variable range of Mach numbers showed the best aerodynamic and dynamic behaviors in comparison with other pellets.

To estimate drag force coefficient, Dali et al. [16], used an axisymmetric 2D Reynolds Averaged Navier-Stokes CFD software at different values of the Mach numbers for three types of projectile caliber 122 mm: a standard projectile (122_ST), a projectile with base bleed called (122_BB), and one with a hollow base shape (122_HB). The GAMBIT software was used to model and grid the 2D body geometry, and afterward, it was exported to the software Ansys Fluent to simulate the airflow around the projectile. The research found that while the base bleed unit provided an improvement in the drag coefficient of 20% compared to the normal bullet, an improvement in the shape of the hollow base was 8%.

Economon et al. [17] investigated a snapshot of ongoing efforts to optimize an open-source CFD analysis and design suite, SU2, for high-performance, scalable Reynolds-averaged Navier-Stokes calculations using implicit time integration. They focused on performance optimizations with a particular emphasis on code profiling, the opportunities for parallelism of the software components, and finding highly-scalable algorithms. Consequently, the resulting code modifications were geared toward achieving coarse- and fine-grained parallelism for edge-based, finite volume CFD solvers, making efficient use of memory within a heavily object-oriented solver, and choosing appropriate algorithms for maximizing parallelism, especially when solving the linear systems arising from implicit time integration of the governing equations.

In the present study, the aerodynamic coefficients acting on 155 mm long-range howitzer ammunition from the Mechanical and Chemical Industry Company (MKEK), which has not been studied in the literature before, along the trajectory followed by subsonic and supersonic velocities in a way that the angle of attack is zero degrees and symmetrical in the x-axis numerically were calculated. To verify the results, the data obtained from the shots made under real physical conditions were compared.

2. EMPIRICAL EQUATION BACKGROUND

There are forces and moments preventing movement in the direction of Cartesian coordinate axes against the 6 DoF movement capabilities of objects moving in an environment using fluid. However, in the trajectory

analysis of the ammunition in this study, the operating directions were accepted as 2D due to the simplified high representation efficiency of the system used. Figure 1 demonstrates the aerodynamic forces which provide lift and drag to the body as it flies through the air in 2D orientation. Here, the velocity and x coordinate components are in the same direction, so the angle of attack is zero.
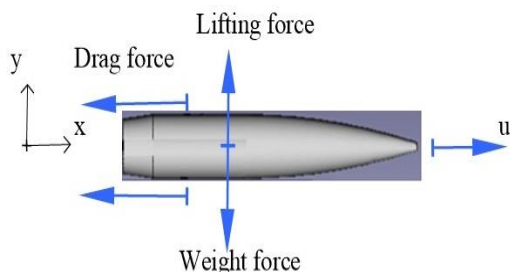
Figure 1. 2D schematic drawing of aerodynamic forces on ammunition.

$$\frac{\partial \rho}{\partial t} + \frac{\partial \rho u_{ij}}{\partial x_{ij}} = 0 \qquad (1)$$

where $\frac{\partial \rho}{\partial t}$ is time deviation of density and $\frac{\partial \rho u_{ij}}{\partial x_{ij}}$ is the convection equation.

The momentum conservation formula in Cartesian tensor notation is as follows:

$$\frac{\partial \rho}{\partial t} + \frac{\partial \rho u_i u_j}{\partial x_j} = f_i - \frac{\partial P}{\partial x_i} + \frac{1}{Re}\left[\frac{\partial \tau_{ij}}{\partial x_j}\right] \qquad (2)$$

where, $\frac{\partial \rho u_i u_j}{\partial x_j}$ is the convection equation, f_i is external force, $\frac{\partial P}{\partial x_i}$ is the pressure gradient, and $\frac{\partial \tau_{ij}}{\partial x_j}$ is shear stress. The energy conservation formula used is:

$$\frac{\partial E_t}{\partial t} + \frac{\partial (u_i E_t)}{\partial x_j} = \frac{-\partial (u_i P)}{\partial x_j} + \frac{-1}{RePr_t}\left[\frac{\partial q_i}{\partial x_j} + \frac{1}{Re}\frac{\partial}{\partial x_j}(u_i \tau_{ij})\right] \qquad (3)$$

where E_t is total energy, Re is Reynolds Number, q_i is heat conduction, τ_{ij} is shear stress and Pr_t turbulent Prandtl number.

The air is compressible during the movement of the ammunition at supersonic Mach numbers, and the simplified versions of the Navier-Stokes equations are realized using Reynolds-Averaged Navier-Stokes (RANS) equations as represented by Eqs. (4) and (5) [18].

$$\frac{\partial \rho}{\partial t} + \frac{\partial \rho u_i}{\partial x_i} = 0 \qquad (4)$$

$$\rho\left(\frac{\partial u_i}{\partial t} + u_j \frac{\partial u_i}{\partial x_j}\right) = F_i - \frac{\partial p}{\partial x_i} \qquad (5)$$

$$+\mu D - u - \rho\left(\partial \frac{-u_i' u_j'}{\partial x_j}\right)$$

$-\rho u_i' u_j'$ is Reynolds Stress

Since the flow is expected to occur with turbulence, the viscosity of the medium will vary. In this case the kinematic eddy viscosity, v_T, an equation for turbulence is written as in Eqs. (6-8) [19].

$$v_T = \frac{a_1 k}{max(a_1 w, S F_2)} \qquad (6)$$

where a_1 is constant that value is 0,31. k is turbulence kinetic energy, w is a specific rate of dissipation and S is strain rate magnitude.

$$F_2 = tanh(arg_2^2)$$
$$arg_2 = max\left(2\frac{\sqrt{k}}{\beta^* wd}, \frac{500\mu}{d^2 w}\right)$$

where d is the distance to the next surface, μ molecular viscosity β^* constant that value is 0,09.

Turbulence kinetic energy and specific dissipation rate equations are as follows:

$$\frac{\partial k}{\partial t} + U_j \frac{\partial k}{\partial x_j} = P_k - \beta^x k w + \frac{\partial}{\partial x_j}\left[(v + \sigma_k v_T) + \frac{\partial k}{\partial x_j}\right] \qquad (7)$$

$$\frac{\partial w}{\partial t} + U_j \frac{\partial w}{\partial x_j} = \alpha S^2 - \beta^x w^2 + \frac{\partial}{\partial x_j}\left[(v + \sigma_w v_T) + \frac{\partial w}{\partial x_j}\right] + 2(1 - F_1)\sigma_{w2}\frac{1}{w}\frac{\partial k}{\partial x_i}\frac{\partial w}{\partial x_i} \qquad (8)$$

σ_k and σ_w turbulent Prandtl number, v_T turbulence viscosity.

$$F_1 = tanh(arg_1^4)$$
$$arg_1 = min\left[max\left(\frac{\sqrt{k}}{\beta^2 wd}, \frac{500\mu}{d^2 w}\right), \frac{4\rho\sigma_{w2}k}{CD_{kw}d^2}\right]$$

where σ_{w2} is constant which is a value of 0,856.

$$CD_{kw} = max\left(2\rho\sigma_{w2}\frac{1}{w}\frac{\partial k}{\partial x_i}\frac{\partial w}{\partial x_i}, 10^{-20}\right)$$

Since the density average changes during the movement of an incompressible fluid, the Navier-Stokes equations (Eqs. 1-3), which take into account the variation of the average density over time, should be simplified with RANS equations (Eqs. 4 and 5) to calculate the turbulence flow. This simplification is achieved by using the Favre Averaged Navier-Stokes (FANS) equations (Eqs. 9-11) [20], which consider the average of mass change of the RANS equations according to time.

$$\frac{\partial \bar{\rho}}{\partial t} + \frac{\partial}{\partial x_i}[\bar{\rho}\tilde{u}_i] = 0 \tag{9}$$

$$\frac{\partial}{\partial t}(\bar{\rho}\tilde{u}_i) + \frac{\partial}{\partial x_j}[\bar{\rho}\tilde{u}_i\tilde{u}_j + \bar{P}\delta_{ij} - \tilde{\tau}_{ij}] = 0 \tag{10}$$

$$\frac{\partial}{\partial t}(\bar{\rho}\tilde{e}_0) + \frac{\partial}{\partial x_j}[\bar{\rho}\tilde{u}_j\tilde{e}_0 + \tilde{u}_j\bar{P} + \tilde{u}_j\bar{P} + \bar{q}_J - \tilde{u}_i\tilde{\tau}_{ij}^{tot}] = 0 \tag{11}$$

$\bar{\rho}$, $\bar{P}$ time-averaged density and pressure, $\tilde{u}$, $\tilde{e}$, τ density averaged velocity, shear stress, and energy

The shear stress sum and its components were written as Eqs. (12-14) [20], which derive from the density averaged momentum conservation Eq. (10).

$$\tau^{\widetilde{tot}} \equiv \tau^{\widetilde{lam}} + \tau^{\widetilde{turb}} \tag{12}$$

$$\tau^{\widetilde{lam}} \equiv \tilde{\tau} = \mu\left(\frac{\partial \tilde{u}_i}{\partial x_j} + \frac{\partial \tilde{u}_j}{\partial x_i} - \frac{2}{3}\frac{\partial \tilde{u}_k}{\partial x_k}\delta_{ij}\right) \tag{13}$$

$$\tau^{\widetilde{turb}} \equiv -\overline{\rho u_i'' u_j''} \approx \mu_t\left(\frac{\partial \tilde{u}_i}{\partial x_j} + \frac{\partial \tilde{u}_j}{\partial x_i} - \frac{2}{3}\frac{\partial \tilde{u}_k}{\partial x_k}\delta_{ij}\right) - \frac{2}{3}\bar{\rho}k\delta_{ij} \tag{14}$$

The total heat equation is given in Eq. 11 and also the components of the energy equation are shown in Eqs. (15–17) [20].

$$q^{\widetilde{tot}} \equiv q^{\widetilde{lam}} + q^{\widetilde{turb}} \tag{15}$$

$$q^{\widetilde{lam}} \equiv \tilde{q}_j \approx -c_p\frac{\mu}{P_r}\frac{\partial \tilde{T}}{\partial x_j} = \frac{-\Upsilon}{\Upsilon-1}\frac{\mu}{Pr}\frac{\partial}{\partial x_j}\left[\frac{\bar{P}}{\bar{\rho}}\right] \tag{16}$$

$$q^{\widetilde{turb}} \equiv c_p\overline{\rho u_j''T} \approx -c_p\frac{\mu_t}{Pr_t}\frac{\partial \tilde{T}}{\partial x_j} = \frac{-\Upsilon}{\Upsilon-1}\frac{\mu_t}{Pr_t}\frac{\partial}{\partial x_j}\left[\frac{\bar{P}}{\bar{\rho}}\right] \tag{17}$$

Again, the average pressure expression used in Eq. (11) is given by Eq. (18) [20].

$$-p = (\Upsilon - 1) - \rho\left(\tilde{e}_0 - \frac{\tilde{u}_k\tilde{u}_k}{2} - k\right) \tag{18}$$

where Υ is the specific heat ratio, c_p specific heat capacity

As a result of the analysis made with RANS and FANS equations, physical quantities such as velocity, pressure, dynamic viscosity, energy, momentum, and density can be calculated.

The friction coefficient (C_d) must be known to calculate the drag force arising directly from the wall shear stress. But this dimensionless coefficient is a function of the air density, drag force which is acting on the object, the speed of the object, and the object's surface area in contact with the air and it is given by Eq. 19 [21].

$$C_d = \frac{2F_d}{\rho A V^2} \tag{19}$$

as the dimensionless concept of C_d is not found directly. If calculated over the drag force:

$$F_d = F_v + F_p \tag{19}$$

where Fv is viscous and Fp is pressure forces. These forces can be calculated using the RANS and FANS equations given by Eq. (4-11). If the found equations are placed in Eq. 19, then the C_d Value can be determined.

3. MATERIAL AND METHOD

The configuration in the present work is designed to determine the drag coefficient related to different Mach numbers. The ammunition used in this study as shown in Figure 2 are 155 mm diameter (d) projectiles with a length of 6.06xd. The rotating band is located at the position of 5.26xd from the nose tip with a width of 0.38xd.

Figure 2. General view of 155 mm (MOD 274) ammunition [22].

The technical properties of the ammunition are displayed in Table 1 [23].

Table 1. Technical properties of 155 mm ammunition.

Weight	43500 g
Length	950 mm
Maximum range	39.000 m
Muzzle velocity	945 m/s

The draft drawing required in the CFD analysis of the real ammunition was created in the FreeCAD environment in a ratio of 1/1 (Figure 3).
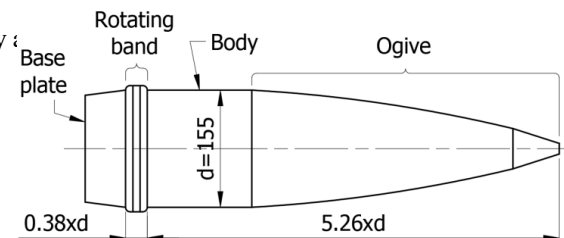
Figure 3. Technical drawing details of 155 mm (MOD 274) ammunition.

The computational domain used was the C-type domain which has a radius of (5xL) and downstream length of (10xL) as shown in Figure 4. The length of the rectangular area was twice the value of its radius and was determined for convergent and accurate results of the

CFD method. The finite area measurements used here were created taking into account the reference [24]. The mesh pattern belonging to the compressible fluid area to be used for the analysis to be made with the SU2 software was performed using the Transfinite method in GMSH software.
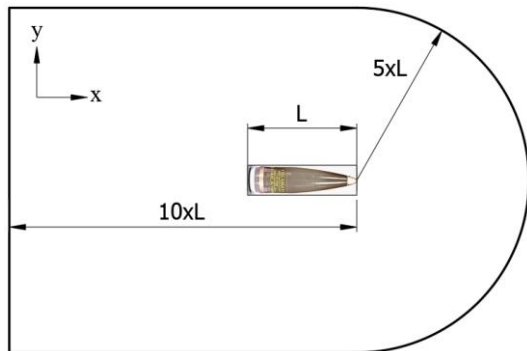

Figure 4. Solution domain dimensions on GMSH.

4. SU2 ANALYSIS and RESULTS

SU2 Computers are used to perform the calculations required to simulate the free-stream flow of fluid and the interaction of fluid (liquids and gases) with surfaces defined by boundary conditions. CFD is a branch of fluid mechanics that uses numerical analyses and data structures to analyze and solve problems that involve fluid flows. One CFD program within SU2 is an open-source finite volume solver program, a software that is used to predict the movement of a 155 mm shell from subsonic to supersonic Mach numbers. The density-based solver and unsteady solution were set in the solver type and were selected for the solution methods. The numerical method for spatial gradient term was computed by the weighted least square cell-based method and the remaining term in the viscosity model used the Sutherland method. Dynamic viscosity is an effective parameter in trajectory analysis of systems in motion at supersonic and transonic speeds. The Sutherland method considers dynamic viscosity as a function of temperature. The turbulent eddy viscosity was calculated from the SST turbulence model. The considered angle of attack was zero degrees for the drag coefficient to calculate the derivative of force, energy, and momentum equations. Other fluid properties such as density, pressure, and temperature were set to standard sea-level conditions. The outer boundaries were set to far-field conditions. The Reynolds number based on the velocity was from 1.65×10^7 to 6.5×10^7 according to the Mach number from 0.7 to 2.8 increasing by 0.3 gradually in the present simulation. Pressure, temperature, density, and energy outputs were obtained as a result of the simulations performed based on the above conditions using SU2 software.

Figure 5 shows the contours of the Mach number in the x-y plane at the conditions of eight different projectile Mach numbers. Here, contours created for only Mach 0.7 and 2.8 are shown, representing the simulation outputs that vary according to Mach numbers. Simulations in each Mach number resulting in 500 iterations in total gave results much closer to drag coefficients at real speed values, with the minimization of errors parallel to the increase in the number of iterations. All simulations were created considering a 10^{-6} margin of error. As expected for all parameters given in Figure 5, it was observed that the pressure waves at Mach 0.7 were formed in the nose of the ammunition. Since the speed of the ammunition in the limited area at this Mach number is approximately 240 m/s, it forces still air into motion. When the velocity of the ammunition is approximately 340 m/s (~1 Mach) and above since the air cannot move faster than the bullet due to its inertia, the air becomes compressed in front of the ammunition, and its density increases. Therefore, parallel to the literature [25], it was determined that the angles of the pressure waves at the ammunition nose level at speeds above Mach 1 decrease due to the compressed and increasing density of the air and that the shock wave curve turns into a narrow-angle starting from the direction of the movement direction and starting from the line of the ammunition nose up to Mach 2.8 supersonic speed. In addition, it was determined that the turbulent flow inclination behind the ammunition, which occurs in the subsonic flow region, is high. As a result, it can be said that there is an inverse proportion between Mach number and shock wave angle. In addition, it can be observed from contour graphs that low-density linear shock waves are formed behind the ammunition parallel to the increase in speed. What is remarkable here is that the waves formed behind the ammunition at low Mach numbers (Mach 0.7) are turbulent. It is believed that ammunition can make pitching movements due to the turbulence that occurs. In simulations, the drag coefficient values calculated by using density-based N-S equations between Mach 1.3 and 2.8 are more accurate, but pressure-based N-S equations were used as well at Mach 0.7 and 1.0.

Similar inferences can be made since the graphs created for energy, pressure, and temperature given in Figure 5 were created using density and pressure-based Navier-Stokes equations.

Percentage changes of density, energy, pressure, and temperature parameters between the minimum and maximum values in simulations, depending on the minimum and maximum Mach number values, are given in Table 2. From this table, it can be observed that the rate of change in parameters increases in parallel with the increase in Mach values at subsonic and supersonic speeds.
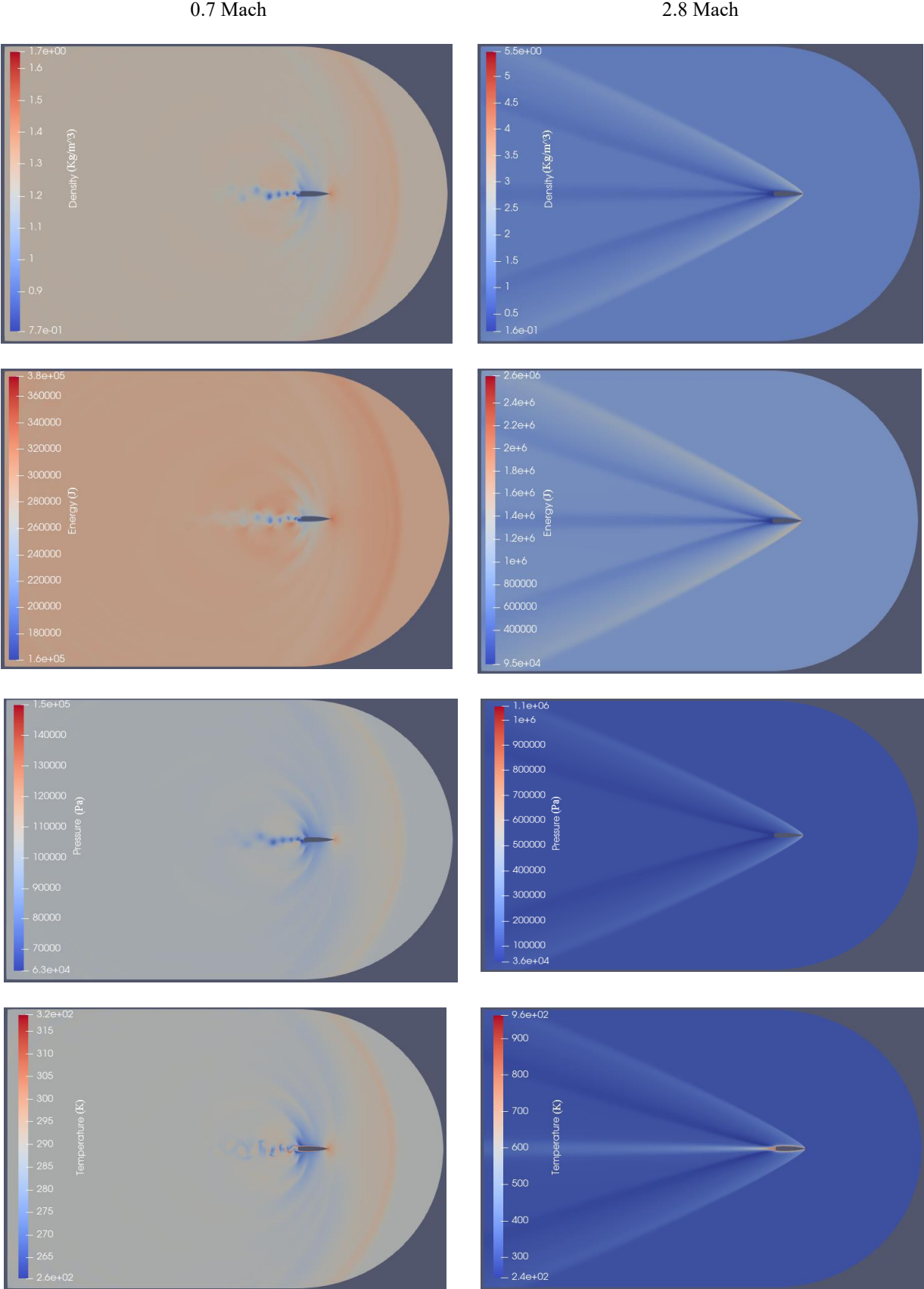
0.7 Mach   2.8 Mach

Figure 5. Contour plots of some properties at Mach 0.7 and 2.8.

Table 2. Percentage change of parameter values due to variation of Mach number

Mach	Density	Energy	Pressure	Temperature
0.7 M	114	132	136	22
1.0 M	329	273	275	68
1.3 M	491	398	398	84
1.6 M	714	582	588	105
1.9 M	1123	906	918	141
2.2 M	1709	1344	1379	191
2.5 M	2156	1974	2016	240
2.8 M	3361	2658	2847	297

Change rates (times) based on Mach numbers			
29.48	20.14	20.93	13.5

Table 3 also includes prediction equations, coefficients of determination (R^2) expressions, and rank values. Initially, to obtain maximum R^2 values, linear, quadratic, logarithmic, and exponential functions were created. Statistically, R^2 is the proportion of the variance in the dependent variable that is predictable from the independent variables. The coefficient of determination normally ranges from 0 to 1 and, if it approaches 1, the representation capability of the equation increases. When the R^2 expressions of the equations created for each parameter are examined, the highest R^2 was obtained in exponential graphs. Accordingly, the R^2 values that provide high consistency in estimating the parameters and the equations they belong to are given in Table 3. When ranking is made, it can be said that the equation with the highest predictive ability is the equation used for density.

Table 3 Prediction equations of aerodynamic parameters.

Equations	$\rho=273.38M^{2.31}$	$E=254.14M^{2.14}$
R^2 (%)	99.09	98.65
Rank	1	2
Equations	$P=257.45M^{2.16}$	$T=50.097M^{1.72}$
R^2 (%)	98.32	96.8
Rank	3	4

In the lowest and highest Mach numbers, the minimum values for each parameter were at the rear of the ammunition, and the maximum values were at the nose. More clearly, the expression of percentage changes and the fit function showing the change and their validity (R^2) can be seen in the graphs given in Figure 6. The proximity of the points given on the graphs to the created curve gives information about the validity of the function used to estimate the parameter. It is seen that the density values, which increase especially according to Mach numbers, have better proximity to the fitted curve compared to the other parameters.
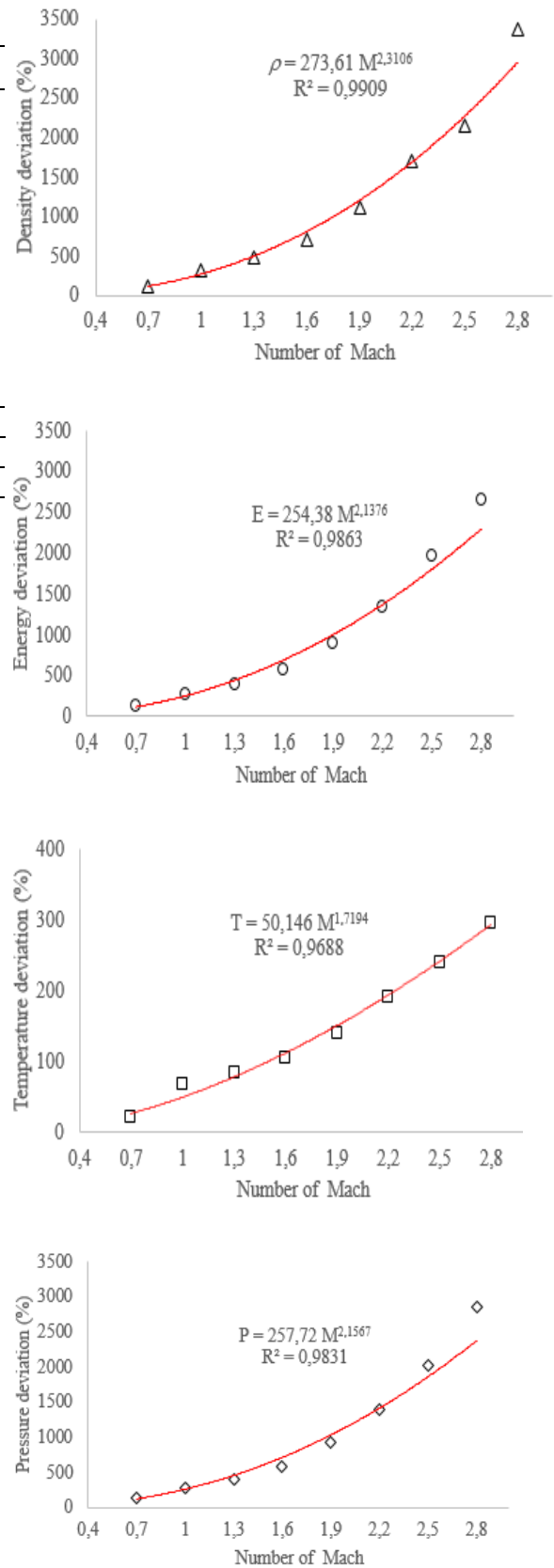
Figure 6. Graphical presentation of percentage change of parameter values.

Since the density and pressure-based RANS equations were used in the energy, pressure, and temperature analyses performed by the SU2 opensource software in the study, R^2 values for these parameters cannot be expected to be higher than the R^2 value formed for the density.

It can be observed that the highest speed of the line slopes between Mach numbers and drag coefficients given in Figure 7 was realized at Mach 2.8. Accordingly, it can be stated that the increasing pressure coefficient caused by the shock wave increases the drag coefficient instantaneously. The geometry of the ammunition is the most important factor affecting the drag coefficient. Similar to what has been seen in the literature, ammunition that is considered to be of ideal geometry will have an instantaneous change in the trajectory geometry, and therefore the drag coefficient, due to the impact of shock waves, especially at high Mach numbers.
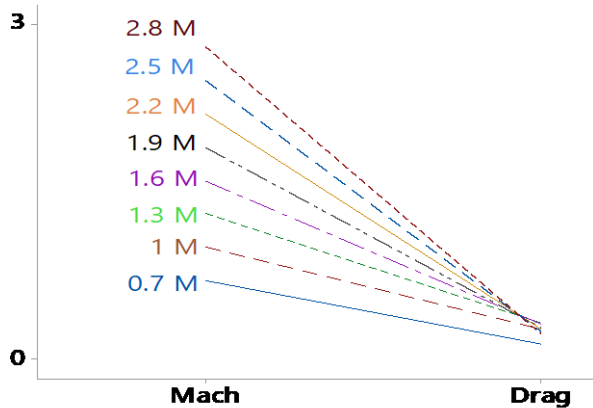

Figure 7. Line plot of Mach vs. drag.

The drag coefficient values of the ammunition used in the SU2 solvent and moving in a compressible medium, whose boundaries are determined with the equations (1-20) given in Chapter 2 within the scope of this article, were simulated at the desired Reynolds and Mach numbers. Figure 8 shows a plot of the drag coefficient with respect to the Mach number from 0.7 to 2.8 at an angle of attack of zero.
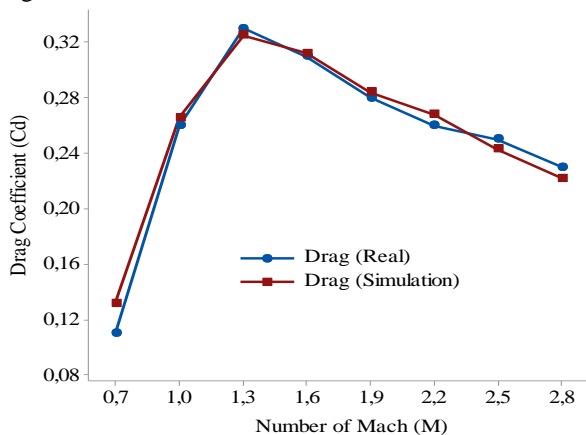

Figure 8. Drag force coefficient (C_d) as a function of Mach number.

The graph shows the drag coefficients generated using the SST turbulence model and the comparison of the drag coefficients obtained using the actual values [26]. According to the graph, it is seen that the drag coefficient shows a sudden increase between Mach 0.7 and 1.3. For this reason, it can be said that the shock waves created by the sound waves occurring in these Mach numbers gather in front of the ammunition, creating a Doppler effect and causing the pressure in front of the ammunition to suddenly increase. At speeds higher than Mach 1.3, the drag coefficient tends to decrease due to the shock waves slowly moving towards the rear of the ammunition. After analysis of the percentage overlap values found by the proportional comparison of the drag coefficient values obtained as a result of the real and simulation results in the same Mach numbers of the graphical data, it was determined that the overlap at Mach 0.7 was 83.33%, and $100 \pm 2\%$ for the other Mach values.

5. CONCLUSION

In this study, RANS equations, operationally simplified variations of the Navier-Stokes flow solver, of 155 mm long-range ammunition, and the aerodynamic properties of the shell were calculated using the computational flow dynamics program SU2. Numerical results were performed with a wide range of Mach numbers and 0-degree angle of attack covering subsonic, transonic, and supersonic flight regions. The results obtained from the CFD analysis made with SU2 software are listed below:

❖ In simulations created according to different Mach numbers for each parameter, it was observed that the margin of error continued to decrease with smaller values after 200 iterations, and it was found that the margin of error was smaller than 10^{-6} after 500 iterations.

❖ It was observed that the shock wave curvature angles at the ammunition nose level at speeds above Mach 1 decreased in the opposite direction to that of movement and, starting from the line of the ammunition nose, turned into a narrow-angle in the same direction at Mach 2.8. Therefore, an inverse proportion can be seen between Mach number and shock wave angle.

❖ For the drag coefficient values, density-based N-S equations for Mach 1.3 and 2.8 and pressure-based N-S equations for Mach 0.7 and 1.0 were found to give more realistic results.

❖ It was determined that the turbulent flow inclination behind the ammunition is high in the subsonic flow region and accordingly, the ammunition may make an undesirable pitching motion.

❖ The density, energy, pressure, and temperature change rates increased parallel to each other due to the increase in Mach values at subsonic and supersonic speeds.

❖ In the lowest and highest Mach numbers used in the study, the minimum values for each parameter were at the rear of the ammunition, and the maximum values were at the nose.

❖ It was seen that the drag coefficient increases sharply between Mach 0.7 and 1.3. At speeds higher than Mach 1.3, it was determined that the drag coefficient tends to decrease due to the shock waves slowly moving towards the rear of the ammunition.

❖ When the percentage overlap values found by the proportional comparison of the drag coefficient values obtained as a result of the real and simulation in the same Mach numbers were examined, it was determined that the overlap at Mach 0.7 was 83.33%, and 100 ± 2% in the other Mach numbers.

Looking at the simulation graphs in all Mach numbers, it was observed that the pressure and temperature were higher in the front of the ammunition. By choosing a rounded design instead of the blunt design of the bullet nose, the airflow can be relieved, and pressure and temperature can be reduced. In this way, a longer range can be achieved as the drag coefficient decreases.

DECLARATION OF ETHICAL STANDARDS
The authors of this article declare that the materials and methods used in this study do not require ethical committee permission and legal-special permission.

AUTHORS' CONTRIBUTIONS
Ahmet Ali SERTKAYA: Performed some simulations. Wrote the manuscript and directed the study.
Can ÇALIŞKAN: Performed all simulations and analyze all results. Wrote the manuscript and directed the study.
Süleyman NEŞELI: Performed some simulations. Wrote the manuscript.

CONFLICT OF INTEREST
There is no conflict of interest in this study.

REFERENCES
[1] Buzan B, Sen G. "The Impact of Military Research and Development Priorities on the Evolution of the Civil Economy in Capitalist States," *Rev Int Stud.*, 1990;16(4):321-339.

[2] Jan TS, Jan CG. "Development of Weapon Systems in Developing Countries: A Case Study of Long Range Strategies in Taiwan," *The Journal of the Operational Research Society,* 2000;51(9);1041-1050. DOI:10.1057/palgrave.jors.2601002

[3] Demir KA. "Challenges Of Weapon Systems Software Development," *Journal of Naval Science and Engineering,* 2009;5(3):104-116.

[4] Bellais R. "Technology and the defense industry: real threats, bad habits, or new (market) opportunities?, " *Journal of Innovation Economics & Management,* 2013;59-78.

[5] Economon TD, Palacios F, Copeland SR, Lukaczyk TW, Alonso JJ. "Su2: an open-source suite for multi-physics simulation and design," *AIAAJ,* 2015.

[6] Economon TD, Mudigere D, Bansal G, Heinecke A, Palacios F, Park J, Smelyanskiy M, Alonso JJ,

Dubey P. "Performance optimizations for scalable implicit RANS calculations with SU2," *Comput Fluids,* 2016;129;146-158.

[7] Guan J, Yi W. "Modeling of Dual-Spinning Projectile with Canard and Trajectory Filtering," *Int J Aerospace Eng.,* 2018; Article ID 1795158.

[8] Suvanjumrat C. "Comparison of turbulence models for flow past NACA0015 airfoil using OpenFOAM," *Eng J-Canada*, 2017;21(3):207-221.

[9] Patel K, Patel S, Patel U, Ahuja AP, "CFD analysis of an Aerofoil," *International Journal of Engineering Research*, 2014;3(33):2319-68902347.

[10] Shen J, Fan S, Ji Y, Zhu Q, Duan J. "Aerodynamics analysis of a hypersonic electromagnetic gun launched Projectile," *Defence Technology*, 2020;16:753-761.

[11] Weinatch P. "Prediction of projectile performance, stability and free flight motion using computational fluid dynamics," *Army Research Laboratory,* 2003; ARL-TR-3015.

[12] Tomasz M, Magier M. "Experimental and numerical analysis of supersonic mortar projectiles," *30th International Symposium On Ballistics Long Beach, Ca,* September 11-15, 2017.

[13] Fonte-Boa R, Borges J, Chaves J. "Analysis of external ballistics for a projectile of caliber 155 mm," *Proelium*, 2017;7:227-241.

[14] Silton SI. "Navier–Stokes Computations for a Spinning Projectile from Subsonic to Supersonic Speeds," *J Spacecraft Rockets*, 2005;42(2).

[15] Rafeie M, Teymourtash AR. "Aerodynamic and dynamic analyses of three common 4.5 mm-caliber pellets in a transonic flow," *Scı Iran,* 2016;23(4):1767-1776.

[16] Dali MA, Jaramaz S, Jerković D, Djurdjevac D. "Increasing the Range of Contemporary Artillery Projectiles," *Teh Vjesn,* 2019; 26(4):960-969.

[17] Economon TD, Palacios F, Alonso JJ, Bansal G, Mudigere D. "Towards high-performance optimizations of the unstructured open-source SU2, Aerospace," *American Institute of Aeronautics and Astronautics*, 2015.

[18] Gal-Chen T, Somerville RCJ. "On the Use of a Coordinate Transformation for the Solution of the Navier-Stokes Equations," *J COMPUT PHYS*, 1975; 17(2):209-228.

[19] Menter FR, Kuntz M, Langtry R. "Ten Years of Industrial Experience with the SST Turbulence Model," *Turbulence, Heat and Mass Transfer*, 4. 2003.

[20] https://www.cfd-online.com/Wiki/Favre averaged _Navier-Stokes_equations Access date:04.01.2021

[21] Sadraey M. Aircraft Performance Analysis. VDM Verlag Dr. Müller; 2011

[22] https://www.standfairoperations.com/products/special-weapons-and-ammunitions/heavy-arms-

ammunition/gun-howitzer-ammunition/155-mm-mke-mod-274-heer-ammunition/

[23] Access date:04.01.2021

[24] https://www.standfairoperations.com/products/special-weapons-and-ammunitions/heavy-arms-ammunition/gun-howitzer-ammunition/155-mm-mke-mod-274-heer-ammunition/ Access date:04.01.2021.

[25] Ko A, Chang K, Sheen DJ, Lee CH, Park Y, Park WS. "Prediction and Analysis of the Aerodynamic Characteristics of a Spinning Projectile Based on Computational Fluid Dynamics," **Int J Aerospace Eng**, 2020; Article ID 6043721.

[26] Becker JV. "The High Speed Frontier: Case Histories of Four NACA Programs," 1920-1950 (NASA History Series Book 445), **National Aeronautics and Space Administration**, 2012; chapter 2, ASIN : B0090SICLW.

Tiryaki E. "Calculation of aerodynamic coefficients, stability properties and trajectory of spin-stabilized projectiles," **Ankara University, Graduate School of Natural and Applied Sciences**, Master Thesis, 2009